



## Nanoindentation on micromechanical properties and microstructure of geopolymers with nano-SiO<sub>2</sub> and nano-TiO<sub>2</sub>

Zhiyu Luo <sup>a</sup>, Wengui Li <sup>a,\*</sup>, Yixiang Gan <sup>b</sup>, Xuzhen He <sup>a</sup>, Arnaud Castel <sup>a</sup>, Daichao Sheng <sup>a</sup>

<sup>a</sup> School of Civil and Environmental Engineering, University of Technology Sydney, NSW, 2007, Australia

<sup>b</sup> School of Civil Engineering, The University of Sydney, NSW, 2006, Australia



### ARTICLE INFO

**Keywords:**  
 Geopolymer  
 Nanoparticle  
 Sodium-aluminium-silicate-hydrate (N-A-S-H)  
 Statistical nanoindentation  
 Nanomodification  
 Microstructure

### ABSTRACT

Fly ash-based geopolymers incorporated with 2% nano-SiO<sub>2</sub> (NS)/nano-TiO<sub>2</sub> (NT) particles were subjected to microstructural and statistical nanoindentation analysis. With the addition of both types of nanoparticles, the compressive strength of geopolymers and the micromechanical properties of N-A-S-H gel were increased. NS exhibited higher reinforcement effect than NT on macro-strength. However, NT more significantly enhanced gel micromechanical properties. NT and especially the NS were found to have a positive effect on the early reaction rate of geopolymers. After 28 days, the gel proportion obtained by Backscattered electron (BSE) images analysis was close values of 49.16%, 55.69% and 54.02% for reference sample and NS, NT reinforced geopolymers, which were more than two times of that from the statistical nanoindentation. The effects of NS and NT on microstructure, gel proportion and gel micromechanical properties were discussed to reveal the macro-strength reinforcement mechanism. The results obtained from different techniques were also compared and discussed.

### 1. Introduction

‘Geopolymer’ is a kind of aluminosilicate binder synthesized by alkaline or alkali-silicate activation of alumina and silica-rich precursor materials [1]. It is well known for the environmental benefit of low carbon footprint. The proper design of geopolymers can make its mechanical properties and durability comparable to Portland cement materials [2]. Great efforts have been made to investigate, understand, optimize and apply this potential green construction material. The optimal design of geopolymers is realized by adjusting alkali solution, source materials, admixtures, related ratio and curing conditions [3], which results in differences in the gel structure, reaction products, degree of polycondensation, etc., and then different properties of geopolymers.

Nowadays, there is an increasing trend to modify and understand materials from the “bottom” scale [4] of nano and even molecular and atomic scale. One of the typical applications in construction materials is nanotechnology, which is defined from two aspects of nanoengineering and nanoscience by Sanchez [5], with the keywords of “manipulation”, “develop” for the former one and “understanding” for the later one. Typical cases for them include modification with nanomaterials and investigation by nanomechanical techniques. Nanomaterials have been

widely studied in Portland cement materials [6–8]. Positive effects including filler effect and nucleation effect of nanoparticles, crack arrest and interlocking effects of two-dimensional nanomaterials, and pozzolanic effect of pozzolanic active nanomaterials have been identified [9, 10], which lead to significant improvements in material properties. Moreover, various nanomechanical testing techniques such as nanoindentation, nanoscratch and modulus mapping have contributed a lot to the understanding of Portland cement materials. There is an increasing trend to combine nanoengineering and nanoscience approaches in research [11–15]. For the application of nanotechnology in geopolymers, relevant studies are insufficient. In addition, the nanomaterial modification and nanomechanical characterization are separate in existing studies. In these limited studies, the benefits of incorporating nanomaterials in geopolymers have also been recognized [16]. Typically, geopolymer strength improvement can be realized by the addition of nano-SiO<sub>2</sub> [17–19], nano-Al<sub>2</sub>O<sub>3</sub> [20], nano-TiO<sub>2</sub> [21], nano-clay [22] and carbon nanotubes [23]. Higher durability such as enhanced sulfuric acid attack resistance of nano-SiO<sub>2</sub> modified geopolymers [17], and lower water absorption of nano-clay modified geopolymers [22] were found. In addition to excellent engineering properties, nanomaterials can help geopolymers gain special properties simultaneously, such as anti-bacterial properties [24] and self-sensing

\* Corresponding author. School of Civil and Environmental Engineering, University of Technology Sydney, NSW, 2007, Australia.

E-mail address: [wengui.li@uts.edu.au](mailto:wengui.li@uts.edu.au) (W. Li).

function [25]. With the deepening of the research on the modification of geopolymer by nanoengineering, it is necessary to promote nanoscience study to help understand the relevant mechanism and lay a basis for further properties improvement.

The most commonly used nanomaterials in cementitious materials are nano-SiO<sub>2</sub> (NS) and nano-TiO<sub>2</sub> (NT) [26], which were adopted in this study to reinforce geopolymer. A high dosage makes it difficult to disperse the nanoparticles, thereby reducing the modification effect and even bringing adverse effects. The optimal dosage of 2 wt% reported previously [17] was applied in this study. The synthesized nano-geopolymer composites were investigated by statistical nano-indentation technique (SNT) to reveal the variation in micromechanical properties of the most crucial phase, sodium aluminosilicate hydrate (N-A-S-H) gel. Besides, X-ray diffraction (XRD) test, Scanning electron microscope (SEM) observation, thermogravimetry analysis (TGA) and hydration heat test were combined conducted for properties investigation and mechanism analysis.

## 2. Experimental program

### 2.1. Material and sample

Class F low calcium Fly ash with the chemical composition listed in Table 1 was adopted as the precursor material. The alkali solution used was a mixture of NaOH solution and Na<sub>2</sub>SiO<sub>3</sub> solution. The NaOH solution was prepared by dissolving NaOH pellets in water. The commercial Na<sub>2</sub>SiO<sub>3</sub> adopted has a silica modulus of 2.07 (14.7% of Na<sub>2</sub>O and 29.4% of SiO<sub>2</sub>). Alkali solutions and fly ash were mixed based on a silica modulus (SiO<sub>2</sub>/Na<sub>2</sub>O) of 1, Na<sub>2</sub>O to ash ratio of 10%, and water to solid ratio of 0.32. The morphology and properties of NS and anatase NT are shown in Fig. 1 and Table 2. They have the same average particle size of 20 nm. Nanoparticles were incorporated by the way of replacing 2% of fly ash while other factors were kept the same as the reference sample. Nanoparticles are easy to combine with each other owing to the high van der Waals force [27]. In this research, 0.5% of Polycarboxylate superplasticizer was incorporated into the alkali solution (also for the reference sample) to help disperse nanoparticles. After adding nanoparticles to the alkali solution, the solution was manually stirred for 3 min and then dispersed in an ultrasonic bath (120 W, 40 kHz) for 2 h. In order to avoid the heat generated in the dispersion process, the water in the bath was replaced every 3 min in the first 1.5 h, every 2 min in the following 20 min and every 1 min in the last 10 min. Alkali solution for the reference sample was also sonicated in the bath.

Geopolymer paste and mortar were mixed by Hobart mixer and cast in 50 mm × 50 mm × 50 mm cubic plastic moulds. In addition to 2 times of sand by weight of fly ash, the mortar samples had the same mix proportions as paste samples. After vibrated for 3 min, samples were sealed by plastic film and cured in a 65 °C oven for 48 h, followed by standard curing until 28 days. Then, small samples with a size of about 10 mm × 10 mm × 5 mm were cut from the core part of geopolymer pastes and embedded in epoxy resin. They were ground by 320, 600 and 1200 grits abrasive papers with each grade lasted for 10 min and polished with a small force by 0.3 µm alumina (for 20 min) and 0.05 µm cerium oxide slurry (for 20 min) to achieve a satisfactory surface. The polished samples were used for the nanoindentation test and BSE image analysis. Besides, paste samples were ground into powders for XRD and TGA analysis. Thereafter, samples were soaked in isopropanol for 3 days and then put in 50 °C vacuum oven drying for 3 days. Prepared samples were stored in a vacuum desiccator.

**Table 1**  
Chemical composition of fly ash.

Oxide	Al <sub>2</sub> O <sub>3</sub>	CaO	SiO <sub>2</sub>	Fe <sub>2</sub> O <sub>3</sub>	K <sub>2</sub> O	MgO	Na <sub>2</sub> O	MnO	P <sub>2</sub> O <sub>5</sub>	TiO <sub>2</sub>	LOI
Weight (%)	25.21	1.73	64.55	2.85	1.47	0.41	0.48	0.07	0.19	0.91	1.54

### 2.2. Compressive strength and workability

For compressive strength, cubic mortar samples were tested at 28 days in accordance with the ASTM C109 (Standard Test Method for Compressive Strength of Hydraulic Cement Mortars) [28]. The workability of fresh geopolymer mortars was tested by flow table test as described in ASTM C1437 (Standard Test Method for Flow of Hydraulic Cement Mortar) [29]. The average result of three samples was reported for tests.

### 2.3. Microcharacterization

The BSE images were taken at the low magnification of 500 × to balance the requirement between details and overall information of samples [30,31]. A total of twenty figures were taken for statistical analysis of each sample. BSE was operated under the accelerating voltage of 15 kV on Zeiss EVO LS15, while Zeiss Supra 55VP was adopted for scanning electron (SE) image observation of geopolymer paste samples to the nanoscale. The voltage for SE observation was 5 or 10 kV. The heat of reaction was measured by TAM Air Isothermal Calorimeter. In order to simulate the heat curing of geopolymer, the temperature condition in the isothermal calorimeter was pre-set and kept at 65 °C for testing. TGA test was conducted by STA449 F5 JUPITER. Vacuum dried powder was heated from 25 °C to 1000 °C with a heating rate of 10 °C/min. The crystals in raw material fly ash and reacted geopolymer were detected by Bruker D8 Discover diffractometer. The step size and 2θ range were 0.02° and 5–70°, respectively.

### 2.4. Statistical nanoindentation technique

Nine of 10 × 10 grids with a grid spacing of 15 µm were performed on samples. In an individual nanoindentation point test, the maximum force was set as 1.5 mN. The loading and unloading time (unloading to 10% of peak force) was 7.5 s. When reaching the maximum force, it was maintained for 5 s to remove creep. Constant Poisson's ratio of 0.2 was set for testing. The modulus and hardness of each point could then be obtained [11]. After deleting abnormal test curves as shown in Fig. 2, the nanoindentation data were subjected to deconvolution analysis.

The distribution of micromechanical properties of geopolymer was described by a two-dimensional Gaussian mixture model (GMM) in Eqs. (1)–(3), where  $x = (M, H)^T$ . M is the elastic modulus and H is the hardness of a test point. Maximum likelihood estimation (MLE) [32–36] is adopted as a deconvolution technique in this study. The parameters of the model including the weighting coefficient, mean value of modulus and hardness and corresponding covariance of phases that can make the log-likelihood function  $\ln L$  given in Eq. (4) achieve the maximum value are the final estimated results. Expectation Maximization (EM) algorithm was used to find the maximum likelihood solution. 1000 times of repeated calculation with random initial input values were made to find the optimum value. After obtaining the estimated model, the testing data was clustered to the corresponding component (phases) based on the maximum posterior probability. In addition, Bayesian Information Criterion (BIC) as shown in Eq. (5) was used to penalize the overfitting errors and find a suitable number of components (phases) to describe the model.

$$p(x) = \sum_{k=1}^K \pi_k \mathcal{N}\left(x \mid \mu_k, \Sigma_k\right) \quad (1)$$

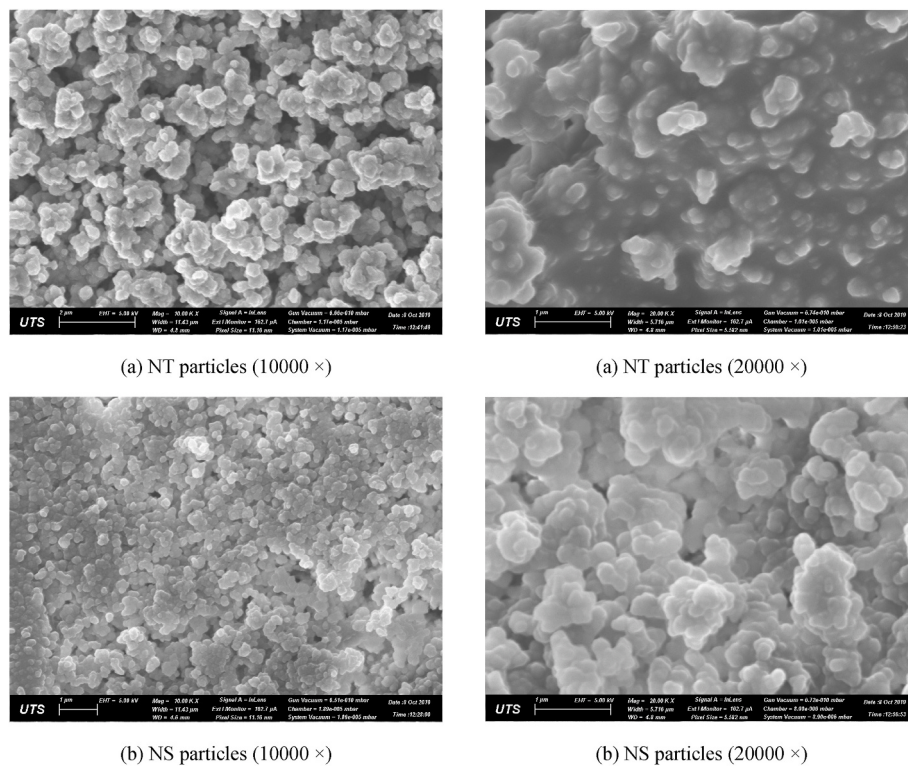


Fig. 1. Morphology of nanoparticles.

**Table 2**  
Basic properties of nanoparticles.

Material	Appearance	Average particle size (nm)	Purity (%)	Type
Nano-TiO <sub>2</sub>	White powder	20	99.9%	Anatase
Nano-SiO <sub>2</sub>	White powder	20	99.9%	Amorphous

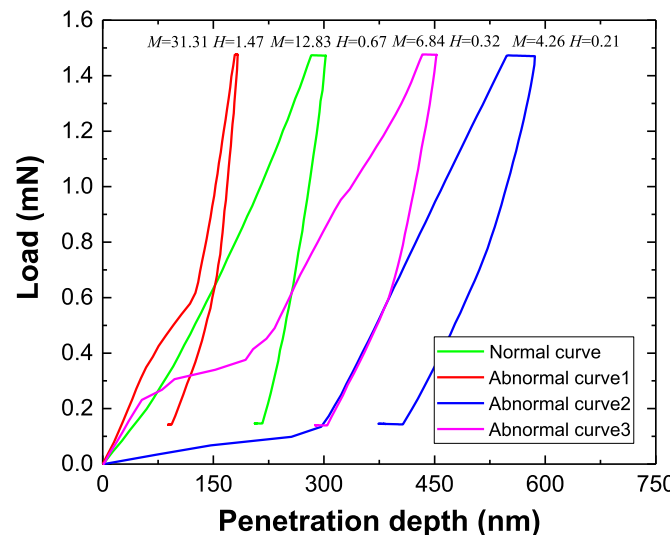


Fig. 2. Typical abnormal nanoindentation test points on sample.

$$\sum_{k=1}^K \pi_k = 1 \quad (2)$$

$$\mathcal{N}(x|\mu, \Sigma) = \frac{1}{\sqrt{\det(2\pi\Sigma)}} \exp\left(-\frac{1}{2}(x-\mu)^T \Sigma^{-1} (x-\mu)\right) \quad (3)$$

$$\ln L = \sum_{n=1}^N \ln \left\{ \sum_{k=1}^K \pi_k \mathcal{N}\left(x_n \middle| \mu_k, \Sigma_k\right) \right\} \quad (4)$$

$$\text{BIC} = k \ln N - 2 \ln L \quad (5)$$

where  $\pi_k$ ,  $\mu_k$  and  $\Sigma_k$  are the weighting coefficient, mean value of modulus and hardness and corresponding covariance of the  $k$ th component, respectively.  $N$  is the number of observed data (nano-indentation test points).

### 3. Results and discussions

#### 3.1. Compressive strength and fresh properties

The 28-day compressive strength of the reference sample, Geo-NS (geopolymer incorporated with NS) and Geo-NT (geopolymer incorporated with NT) are  $30.5 \pm 1.31$  MPa,  $35.8 \pm 1.12$  MPa and  $33.7 \pm 0.83$  MPa, respectively. It means that both NS and NT particles have enhanced the strength of geopolymers, with an improvement of 17.38% and 10.49% for Geo-NS and Geo-NT samples, respectively. The addition of nanoparticles shows a slightly adverse effect on the workability, owing to the high specific area of fine particles. The flow diameter for the reference sample was 152.3 mm, while a smaller diameter of 148.4 mm and 145.7 mm were observed for Geo-NS and Geo-NT mortar samples. Due to the use of superplasticizer, the nano-geopolymers still have good workability.

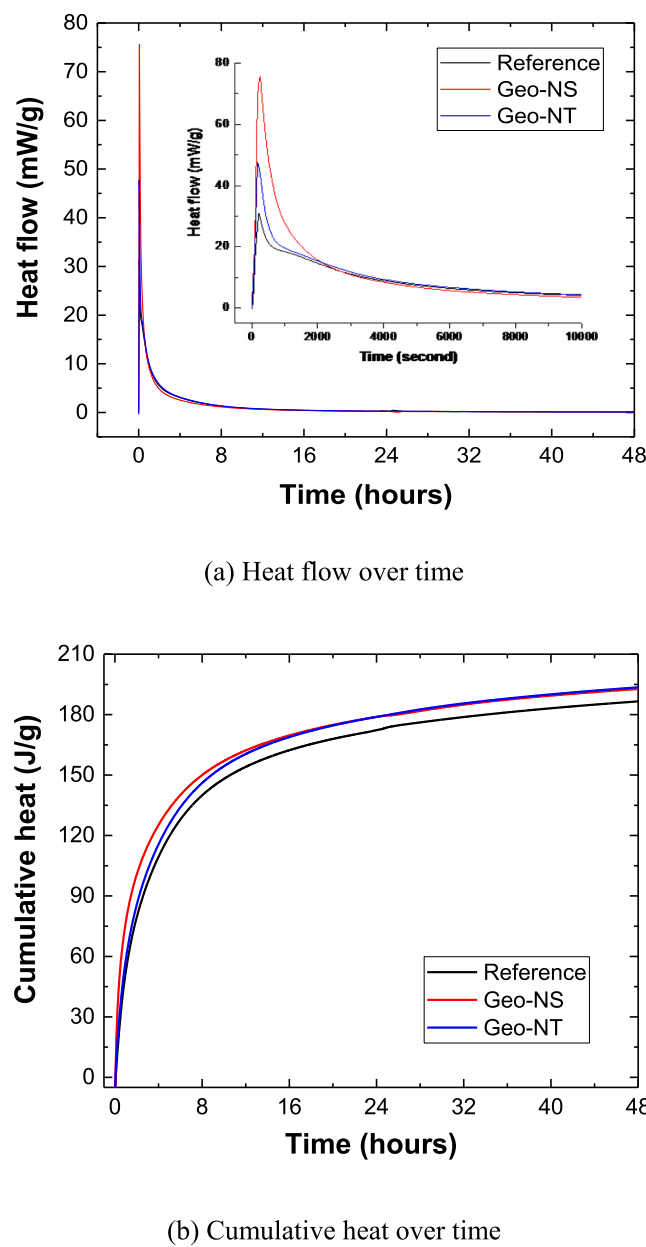


**Fig. 3.** Heat of reaction during the first 48 h.

### 3.2. Heat of reaction

The heat of reaction of samples during the first 48 hr is given in Fig. 3. As presented in Fig. 3(a), the heat flow curves are similar for these three samples. When compared with Portland cement paste [37], much higher heat flow is found for the heat cured geopolymers in the initial stage, and no peak was obtained in the later stage. The detailed figure in Fig. 3(a) indicates that the highest heat release rate occurs at a similar time for samples. The nanomodified samples show significantly higher heat flow than the reference sample in the initial 2000 s, with the highest value achieved by Geo-NS. It indicates that NT and especially NS have accelerated the reaction rate, quite similar to the phenomenon observed in Portland cement paste [6,38,39]. It would be attributed to increased interparticle space [40], as well as the possible nucleation effect from the ultra-small size of particles [39,41–43]. Increased thermal conductivity could also contribute to the acceleration of reaction. However, considering the fact that NT with high thermal conductivity than NS brings a less significant increase in the heat flow of geopolymer, this

factor should be less dominant than others in the initial stage. In terms of the cumulative heat generated, similar values were achieved for Geo-NS (193.56 J) and Geo-NT (193.95 J) samples, all larger than the reference sample (186.64 J). The higher cumulative heat in the nanomodified samples implies the higher reaction degree promoted by both nanoparticles during the first 48 hr. A previous study for nano-Al<sub>2</sub>O<sub>3</sub> indicated that it can avoid the induction period in NaOH activated fly ash, generating gel much earlier [43]. Thus, the results for NS and NT again reveal the potential of nanoparticles for improving the early performance of geopolymer, which is in agreement with macro-mechanical results [21,44].

### 3.3. Micro and nanoscale structure of geopolymer paste

The micro and nanoscale structure of geopolymers is shown in Fig. 4. At the magnification of 5000×, Fig. 4(a) shows that geopolymer is mainly composed of residual fly ash and matrix. Defects such as pores and cracks are found to present in both fly ash and matrix. At the higher magnification of 10000×, the local microstructure observation of matrix in Fig. 4(b) indicates that in addition to the main reacted product of N-A-S-H gel, sometimes there are also microcrystals. At this magnification, the image starts to show the feature that the matrix generated has a looser microstructure than the raw materials fly ash. The nanoscale's images can more clearly reveal the difference. In Fig. 4(c), the N-A-S-H gel in matrix is found to be a loose structure packed by different particles, while the appearance of the fly ash (upper right corner) is still smooth and dense at this magnification. Nanoscale's details of the matrix are displayed in Fig. 4(d). The particles pile up and entangle with each other. Most of them display in the granular form. Some typical particles displayed are found to have a size of slightly more than 30 nm. It should be noted that these particles actually consist of smaller globules as the basic unit. Due to the resolution limitation of SEM techniques, the smaller globules can be just seen faintly in the enlarged picture of 300000×, which are reported to have a size of around 5 nm [1].

### 3.4. Crystals in geopolymer

The crystals detected by XRD are presented in Fig. 5. Quartz and Mullite are the main crystals in geopolymer. Compared with the raw material fly ash, it shows that there is no new kind of crystal generated in the activated system, which is in line with some previous studies [1]. The geopolymer aluminosilicate gel has been proposed to be related to the precursor gel for the formation of zeolite [1]. The new zeolite phase Na-F was formed in the nano-Al<sub>2</sub>O<sub>3</sub> seeded geopolymer [43]. However, a previous study for geopolymer incorporated with Zirconia showed that it is not able to act as a nucleation germ for zeolite formation [45]. The XRD analysis in this research reveals that the NS and NT also fail to promote the evolution of the zeolite phase.

### 3.5. Micromechanical properties and proportion of nano-reinforced N-A-S-H gel

#### 3.5.1. Spurious phases and a compromise strategy for deconvolution

Geopolymer is mainly composed of N-A-S-H gel, unreacted fly ash, pores/cracks and crystals. However, the deconvolution of the Gaussian mixture model would not be able to accurately obtain the distribution of micromechanical properties of all phases [32]. Spurious phases such as mixed phase and sub-phases would be generated owing to the combined effects of phase characteristics, test factors, deconvolution parameters, etc. In the nanoindentation test, the involved range of gel is 3–4 times of the penetration depth [46]. Thus, the test results of nanoindentation sometimes come from multiphase interactions, such as interactions between gel and microcrystalline, gel and fly ash. These test points are one of the sources of the spurious phases. Typically, because of the small size of the crystal phase, most of the test results for it actually come from the composite response of the crystal and gel.

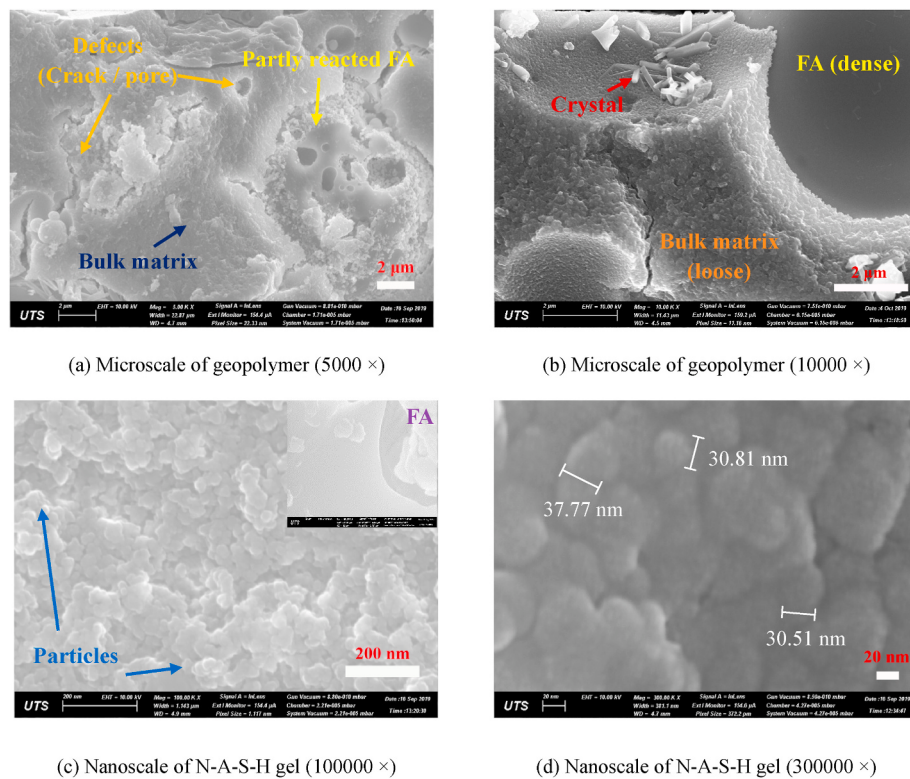


Fig. 4. Microstructure observation of geopolymers paste.

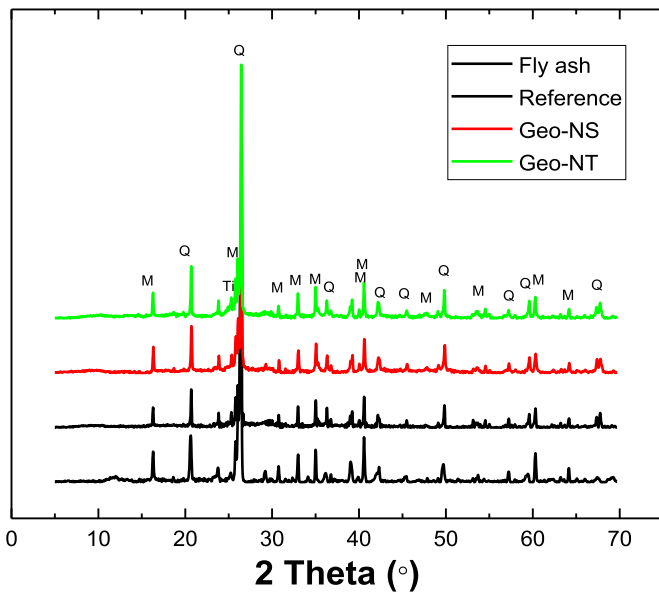


Fig. 5. XRD results of nanoparticles reinforced geopolymers paste.

For the nanoindentation data collected, the deconvolution analysis would play a very important role in presenting micromechanical information of phases. When the number of phases specified is small, the deconvolution result of phases would be a mixture of multiple phases (mixed phases caused by deconvolution). However, increasing the number of phases in the model would sometimes lead to sub-phases. For instance, Phase like fly ash has a wide range of micromechanical distribution especially when pores are presented. Its micromechanical distribution is sparse at some locations and would sometimes overlap with other phases (crystals and mixed phases from multiphase

interactions). As a consequence, some fly test data would be misidentified as individual phases (sub-phases) or incorporated into other phases in deconvolution. The mixed phases and sub-phases would exist in the deconvolution model simultaneously. In lots of the case of deconvolution, the sub-phases of fly ash occur before obtaining the gel phase from the mixture of multiple phases. Therefore, the micromechanical properties of the gel phase and fly ash cannot be accurately obtained at the same time. Additionally, the small amount of the real test points on the crystal phase makes it very easy to be combined with others with similar micromechanical properties in deconvolution instead of presence as an individual peak. The real micromechanical properties of the crystal phase are almost impossible to be obtained from the deconvolution analysis. Considering the above issues, a compromise strategy [32,33] is adopted. The micromechanical investigation in this study just focuses on the most crucial phase, N-A-S-H gel.

**Table 3**  
Micromechanical properties of Geo-NT.

k	M [GPa]	H [GPa]	f	BIC	C		
					C11	C12 = C21	C22
3	19.25	1.15	47.42%	9151.100	31.31	1.53	0.14
4	19.30	1.15	47.76%	9094.102	31.77	1.54	0.14
5	18.73	1.13	44.78%	9055.36	27.58	1.37	0.13
6	15.44	0.90	24.67%	9029.64	11.43	0.49	0.06
7	14.68	0.86	18.93%	9026.98	9.33	0.41	0.05
8	15.39	0.90	24.63%	9019.36	11.20	0.48	0.06
Average	15.17	0.89	22.74%	–	10.65	0.46	0.06
6-8							

Note: Geo-NT is 2% NT modified geopolymers with 65 °C heat curing of 48 hr k is the number of phases. "M" and "H" refer to mean value of elastic modulus and hardness, respectively. f is the proportion of the phase. C11 is the variance of elastic modulus, C22 is the variance of hardness and C12 is the covariance of modulus and hardness.

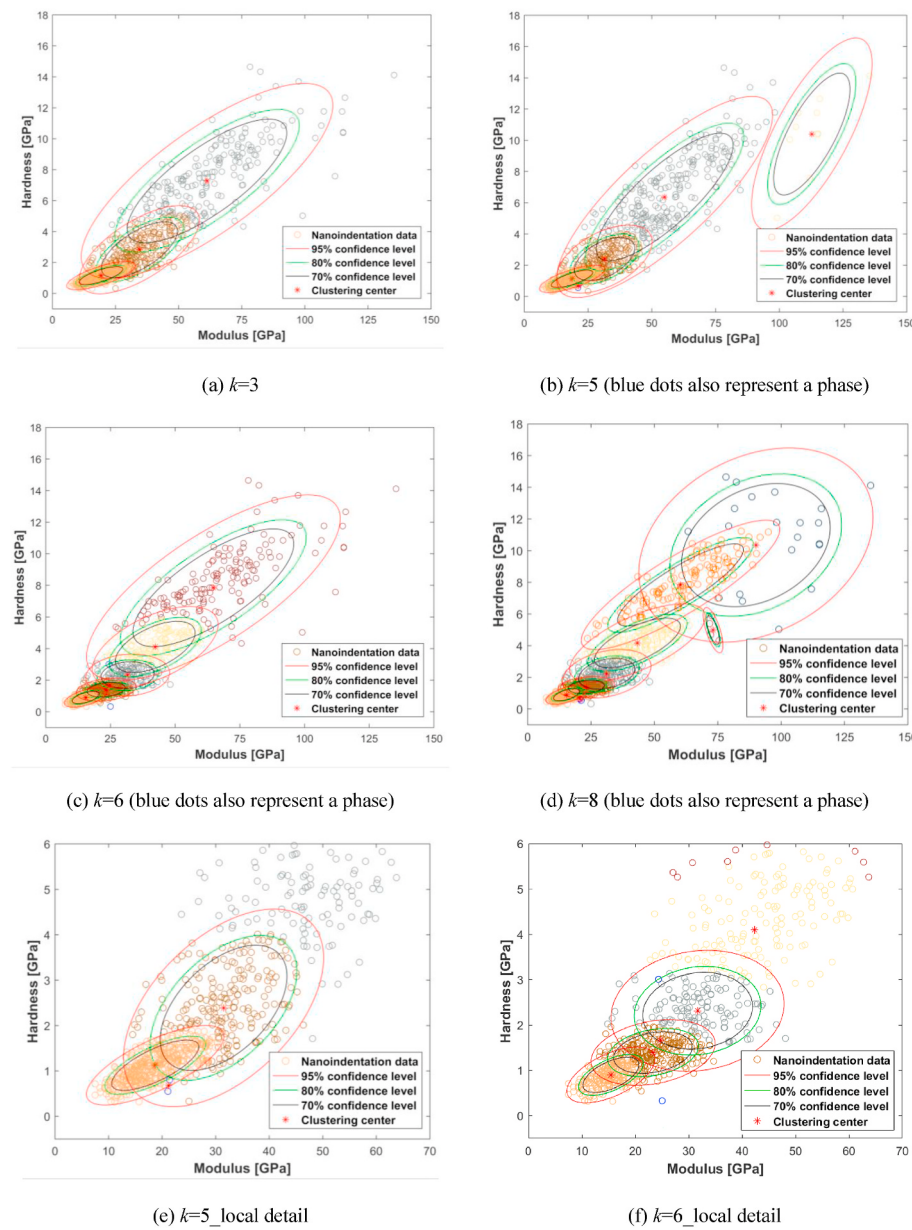


Fig. 6. Statistical nanoindentation results for Geo-NT.

### 3.5.2. Micromechanical properties of nano-reinforced N-A-S-H gel

The deconvolution process is briefly illustrated based on the case of Geo-NT. As shown in Table 3 and Fig. 6, for the model of Geo-NT with 3 phases, it is the sand brown phase that has the minimum micromechanical properties, with the modulus of 19.25 GPa, hardness of 1.15 GPa and covariance matrix of ( $C_{11} = 31.31$ ,  $C_{12}=C_{21} = 1.53$ ,  $C_{22} = 0.14$ ), respectively. When increasing the number of phases to 4 and 5, there is no significant change for the sand brown phase. For this phase, it has high micromechanical properties and especially large variance, which does not conform to the characteristics of the gel phase [32–34, 36]. The N-A-S-H gel phase with small micromechanical properties ( $M = 15.44$  GPa,  $H = 0.90$  GPa) and small covariance matrix ( $C_{11} = 11.43$ ,  $C_{12}=C_{21} = 0.49$ ,  $C_{22} = 0.06$ ) appears when the number of phases was set as 6, which changes just slightly with the increase in the number of phases. The decomposition of the above sand brown phase to the new smaller sand brown phase (N-A-S-H) can be observed clearly in Fig. 6 (b)–(c) and (e) to (f). However, the BIC does not reach the optimal value (minimum value) even if 7 components are assigned to the model as shown in Table 3. As mentioned above, there are two kinds of spurious

phases, mixed phase and sub-phase. In the deconvolution analysis, with the increase in the number of phases, the mixed phases would decrease while the sub-phases would increase. It is obvious that sub-phases (e.g. phase with  $M$  of 112.79 GPa and  $H$  of 10.39 GPa) already present in the model with 5 components while the sand brown phase is still the mixture of gel and other phases. The scattered test points of fly ash make the spurious sub-phases evaluated as reasonable by the mathematical method of BIC, but does not conform to the real distribution. Therefore, it is not feasible to obtain the optimum model by BIC to analyze the properties of N-A-S-H gel because the excessive separation of phases is wrongly evaluated as reasonable. Besides, the normally used 4 components in deconvolution would make the result actually the mixture of gel and other phases. The compromise strategy of studying the N-A-S-H gel merely instead of all of the phases can avoid these problems. The micromechanical properties of N-A-S-H are determined by the average value of the N-A-S-H phase in the first three models as shown in Table 3. The elastic modulus, hardness and proportion of N-A-S-H gel in Geo-NT are 15.17 GPa, 0.89 GPa and 22.74%, respectively.

For reference and Geo-NS sample, the N-A-S-H gel appears in model

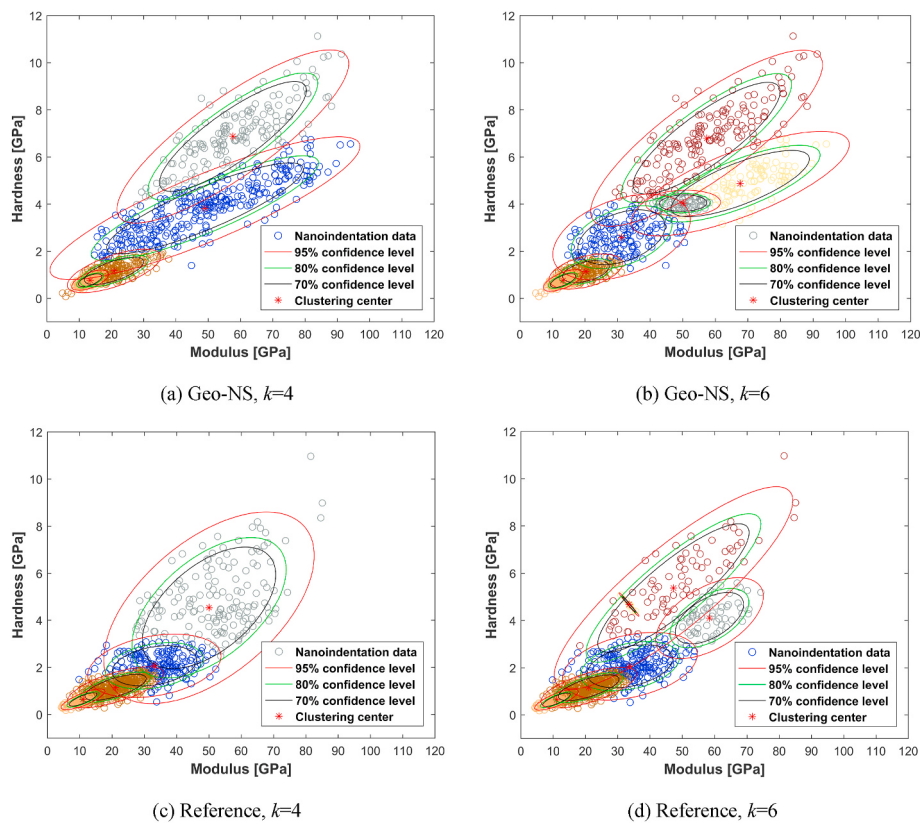


**Fig. 7.** Statistical nanoindentation results for Geo-NS and reference sample.

**Table 4**  
Micromechanical properties of Geo-NS.

<i>k</i>	<i>M</i> [GPa]	<i>H</i> [GPa]	<i>f</i>	BIC	C		
					C11	C12 = C21	C22
4	13.38	0.76	22.80%	9051.71	5.47	0.25	0.03
5	13.27	0.75	24.36%	9020.92	6.27	0.31	0.04
6	13.26	0.75	24.19%	9001.09	6.23	0.3	0.04
Average	13.30	0.75	23.78%	–	5.99	0.29	0.04

Note: Geo-NS is 2% NS modified geopolymers with 65 °C heat curing of 48 h *k* is the number of phases. “*M*” and “*H*” refer to mean value of elastic modulus and hardness, respectively. *f* is the proportion of the phase. C11 is the variance of elastic modulus, C22 is the variance of hardness and C12 is the covariance of modulus and hardness.

**Table 5**  
Micromechanical properties of the reference sample.

<i>k</i>	<i>M</i> [GPa]	<i>H</i> [GPa]	<i>f</i>	BIC	C		
					C11	C12 = C21	C22
4	11.04	0.64	12.20%	8341.59	7.78	0.40	0.03
5	11.02	0.64	12.15%	8297.51	7.74	0.40	0.03
6	11.02	0.64	12.13%	8278.39	7.74	0.40	0.03
Average	11.03	0.64	12.16%	–	7.75	0.40	0.03

Note: *k* is the number of phases. “*M*” and “*H*” refer to mean value of elastic modulus and hardness, respectively. *f* is the proportion of the phase. C11 is the variance of elastic modulus, C22 is the variance of hardness and C12 is the covariance of modulus and hardness.

with 4 components, and behaviours as a stable phase with the increase in the number of components. The model and SNT results for Geo-NS and reference with 4 and 6 components are shown in Fig. 7 as well as

Tables 4 and 5, respectively. The average elastic modulus, hardness and proportion of N-A-S-H gel in Geo-NS are 13.30 GPa, 0.75 GPa and 23.78%, respectively. The corresponding values in the reference sample are 11.03 GPa, 0.64 GPa and 12.16%, respectively.

### 3.5.3. Repeatability and validity of gel proportion and micromechanical properties

According to the above results, it is clear that the nanoparticles would increase the micromechanical properties of the gel, and the Geo-NT achieves the highest value. Besides, the proportion of gel for the reference sample is just about 50% of the Geo-NT and Geo-NS samples. Before using the above results to analyze the micro mechanism of the macro properties, verification was conducted to understand the repeatability and validity of the results.

Since the reference sample has the lowest gel proportion, SNT test was conducted on the sample again to investigate if the results were affected by limited test points and also the repeatability of SNT results. For the above results of reference, Geo-NT and Geo-NS, they were based on the random principle of the SNT, namely, each grid was selected randomly. Since the research focusing on the gel phase only, grids nanoindentation were performed on gel rich areas to provide richer test data and more accurate test results for gel. In the repeated test procedure, six locations were selected randomly under a microscope and then grids were intentionally set on the gel rich area within the field of vision. The test result is provided in Fig. 8 and Table 6. Regarding the verification of proportion, BSE images were taken. These images were segmented into three phases of pores/cracks, gel and unreacted fly ash as shown in Fig. 9. The proportions of the gel phase determined by BSE and by nanoindentation are summarized in Table 7.

As shown in Table 7, the SNT results based on 12.16% gel and 31.01% gel data set in different tests are quite similar to each other. It means that the accuracy of the test method would not be a significant obstacle for the comparison of micromechanical properties. However,

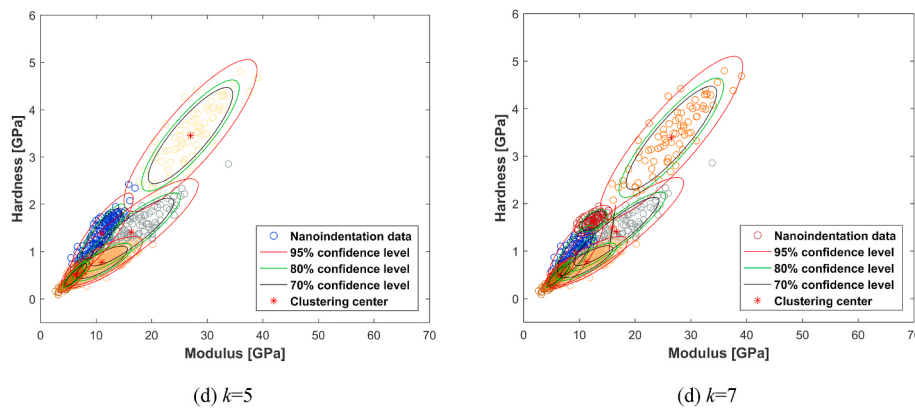


Fig. 8. Statistical nanoindentation results for Reference-repeated.

**Table 6**  
Micromechanical properties of reference sample-repeated.

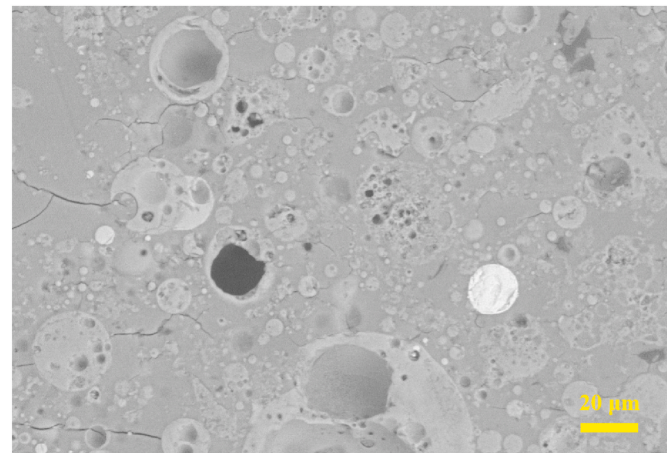
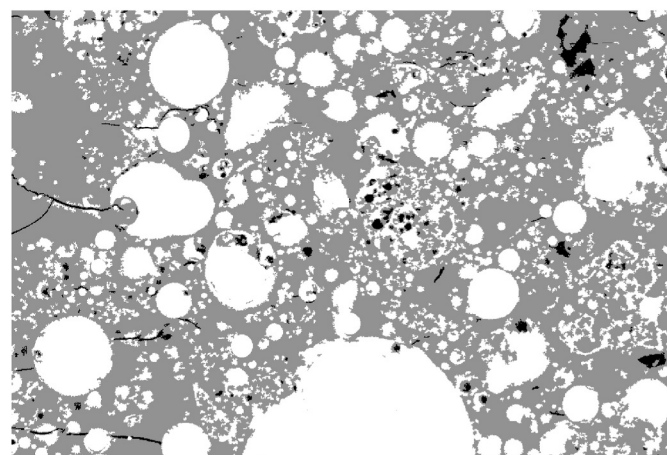
$k$	$M$ [GPa]	$H$ [GPa]	$f$	BIC	$C$		
					$C_{11}$	$C_{12} = C_{21}$	$C_{22}$
5	11.07	0.78	33.42%	4991.91	8.88	0.52	0.05
6	11.30	0.77	29.89%	4972.91	9.03	0.54	0.05
7	11.32	0.77	29.71%	4960.76	9.10	0.54	0.05
Average	11.23	0.77	31.01%	—	9.00	0.53	0.05

Note:  $k$  is the number of phases. “ $M$ ” and “ $H$ ” refer to mean value of elastic modulus and hardness, respectively.  $f$  is the proportion of the phase.  $C_{11}$  is the variance of elastic modulus,  $C_{22}$  is the variance of hardness and  $C_{12}$  is the covariance of modulus and hardness.

the gel proportion obtained by statistical nanoindentation is obviously different from that obtained by the generally used BSE technique. In this study, epoxy resin was not used to impregnate the surface to avoid its effect on micromechanical testing. Thus, crystals are basically dropped, making the gel proportion obtained by BSE greater than the true value. However, since crystals in matrix may be mainly from raw material fly ash, the interference would not impact the relative trend of gel proportion significantly. BSE would still be a more accurate method than SNT on phase proportion evaluation as analyzed in the next section. Based on the result of BSE, and considering that nanoparticles are added in a way of replacing FA, the difference of gel content in samples should be small.

### 3.6. Microscale mechanism of macro performance

As opposed to the phenomenon at the macro scale where Geo-NS displays better performance than others, it is the gel in Geo-NT that has the highest modulus and hardness. Besides, for random nanoindentation results, the reference sample presents only 12.16% of gel while Geo-NT and Geo-NS have 22.74% and 23.78% gel, respectively. If based on the SNT results solely, it is easy to consider that the nanoparticles have increased the content of the gel/reaction degree and then better macro performance. In fact, the number of nanoindentation test points is very few when compared with pixels in BSE images, which is hard to accurately reflect the overall information of the highly heterogeneous geopolymers. Besides, the interaction of gel with other phases in the involved volume would also decrease the proportion of gel detected by deconvolution analysis. Therefore, the proportion obtained from SNT should be less reliable than that from BSE. More evidence is the TGA result as shown in Fig. 10. The remaining weights for reference, Geo-NS and Geo-NT are 88.55%, 88.98% and 88.82%, respectively. The weight loss between 25 and 300 °C is the free water and loosely bound water, while the weight loss in the later period is caused by the loss of structure

(a) BSE image ( $500 \times$ )

(b) Segmented image

Fig. 9. Segment of phases based on the grey value of BSE image.

water and carbonaceous substances [47]. When the influence of free water is eliminated, the TGA results are almost the same for all the specimens, indicating that there would be no significant difference between the content of the gel phase.

As analyzed through the heat of reaction, the nanoparticles have an accelerating effect in the early stage. It would lead to a higher amount of

**Table 7**  
Summary of results from SNT and BSE.

Samples	Modulus (GPa)	Hardness (GPa)	Proportion from SNT	Proportion from BSE
Geo-NT	15.17	0.89	22.74%	54.02%
Geo-NS	13.30	0.75	23.78%	55.69%
Reference	11.03 (11.23)	0.64 (0.77)	12.16% (31.01%)	49.16%

Note: Samples were heat cured at 65 °C for 48 h. The results in brackets are from the repeated test on the reference sample where some grids are intentionally set on gel rich area.

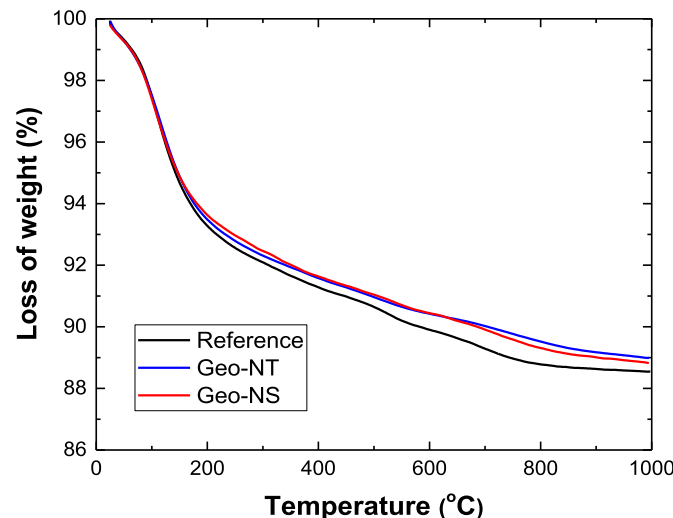


Fig. 10. Thermogravimetric analysis of geopolymer paste.

gel in nano-geopolymers, which plays a significant role in the early performance of geopolymer. In fact, both NT and NS particles in this study could be treated as unreactive particles due to the limited solubility of NS in the sodium silicate solution. These particles promote the growth of gel in a more physical way, just as the interparticle distance is demonstrated as the most important parameter for the mineral additions to accelerate the clinker hydration [40]. Therefore, the relative difference of gel content (not the absolute difference) between geopolymer and nanomodified geopolymer would narrow over time. For the later stage, instead of the gel proportion, the differences in macro-mechanical properties between samples would be more related to the strength of the gel, as well as the coordination (e.g. bonding) between gel and other phases.

For nano-geopolymer, the nanoparticles could act as filler which contributes to the formation of a denser gel structure and then improved macro behavior. However, the NS would be more compatible with both sodium silicate solution and N-A-S-H gel particles due to the similar chemical composition. The NS may achieve better dispersion and also integrate with the N-A-S-H gel particles better, resulting in more prominent macro mechanical properties. For micromechanical properties, the denser gel structure would also result in higher modulus and hardness. However, there is another factor that would influence the micromechanical results significantly.

In the nanoindentation test, the involved depth is usually considered as 3 to 4 times of the indentation depth [46], reaching around 1 μm on N-A-S-H gel. When the nanoparticles are well dispersed (single particle, very small aggregations), they have a similar size to the gel particles shown in Fig. 4(d), and works together with the gel particles as a composite. Owing to the large involved range, the well-dispersed nanoparticles are able to be detected by the nanoindentation test. The micromechanical properties of N-A-S-H in nano-geopolymers come from the interaction of gel particles and nanoparticles. Single nanosilica is

reported to have elastic modulus and hardness of  $68.9 \pm 9.6$  GPa and  $2.8 \pm 0.4$  GPa, respectively in nanoindentation test [48]. For nano-titania (anatase), the modulus and hardness are as high as around 170 GPa and 8 GPa, respectively [49,50]. N-A-S-H gel is actually similar to the counterpart LD C-S-H gel. Both are reported to consist of globules of about 5 nm [1,51]. The nanoindentation results for them are also quite close. The globules of C-S-H are reported to have an elastic modulus of  $59.7 \pm 1.9$  GPa [52]. Therefore, the N-A-S-H gel particles with a size larger than 30 nm would have a smaller elastic modulus due to the existence of nanopores between the packed globules. The higher mechanical properties of NS and especially NT particles than gel particles contribute to the high micromechanical properties of nano-reinforced N-A-S-H gel detected. Meanwhile, because of the small size and small proportion of the nanoparticles in each test point, the SNT results of the nano-reinforced gel would be improved but within a small range. For some of the nanoparticles that happen to present densely in the nanoindentation test points (poor dispersion), these test points with significantly high mechanical properties would not be identified and clustered to the gel phase in the deconvolution process. The above reasons lead to the results in Table 7 for the gel particles-nanoparticles composites where Geo-NT and reference sample achieve the highest and the lowest value, respectively. Thus, the properties of the particles themselves cause the different reinforcement effect of NS and NT on macro compressive strength and micro modulus and hardness.

#### 4. Conclusions

The effect of the nanosilica (NS) and nano titanium dioxide (NT) particles on the microscale properties of geopolymer, especially the most important component N-A-S-H gel, was investigated to promote the understanding of the reinforcement mechanism of different nanoparticles. Conclusions can be drawn up as follows:

- (1) The addition of 2% nano-SiO<sub>2</sub> and nano-TiO<sub>2</sub> particles helps the geopolymers gain 17.38% and 10.49% in strength at 28 days but leads to a slight decrease in workability.
- (2) The content of the N-A-S-H gels obtained by SNT vary significantly for samples and are less than around 50% of the BSE results. SNT results due to the limited test points on the highly heterogeneous geopolymer are considered less reliable than the results from BSE. Besides, the multiple phase interaction would be responsible for the significantly lower amount of gel detected by SNT.
- (3) The presence of both nano-SiO<sub>2</sub> and nano-TiO<sub>2</sub> particles increase the early reaction rate in geopolymer, while the reaction degree of different samples in the later age is not vastly different. The contents of gel in 28 days geopolymer and nano-geopolymers vary in a small range of 49.16%–54.02%.
- (4) Gel particles packed by around 5 nm globules are typically observed to have a size of more than 30 nm, similar to the size of well-dispersed nanoparticles. Nanoparticles integrate with gel particles to form a composite with higher mechanical properties. The elastic modulus of N-A-S-H gel is 11.03 GPa, 13.30 GPa and 15.17 GPa, respectively, for reference, Geo-NS and Geo-NT sample.
- (5) Nanoparticles have higher mechanical properties (highest for NT) but a much lower proportion than the gel particles, leading to slightly higher micromechanical properties of gel in nano-geopolymers obtained by SNT. Nano-SiO<sub>2</sub> is more compatible with sodium silicate solution and gel particles, resulting in better dispersion and bonding, then a higher macro strength of Geo-NS than Geo-NT.

#### Declaration of competing interest

The authors declare that they have no known competing financial

interests or personal relationships that could have appeared to influence the work reported in this paper.

## Acknowledgement

All authors appreciate the supports from the Australian Research Council (ARC) (DE150101751 and IH150100006), University of Technology Sydney Research Academic Program at Tech Lab (UTS RAPT), and University of Technology Sydney Tech Lab Blue Sky Research Scheme. The first author would like to thank the support by the Australian Government Research Training Program Scholarship.

## References

- [1] J.L. Provis, G.C. Lukey, J.S. van Deventer, Do geopolymers actually contain nanocrystalline zeolites? A reexamination of existing results, *Chem. Mater.* 17 (12) (2005) 3075–3085, <https://doi.org/10.1021/cm050230i>.
- [2] S.A. Bernal, J.L. Provis, Durability of alkali-activated materials: progress and perspectives, *J. Am. Ceram. Soc.* 97 (4) (2014) 997–1008, <https://doi.org/10.1111/jace.12831>.
- [3] D. Khale, R. Chaudhary, Mechanism of geopolymerization and factors influencing its development: a review, *J. Mater. Sci.* 42 (3) (2007) 729–746, <https://doi.org/10.1007/s10853-006-0401-4>.
- [4] R.P. Feynman, There's plenty of room at the bottom, *Eng. Sci.* 23 (5) (1960) 22–36.
- [5] F. Sanchez, K. Sobolev, Nanotechnology in concrete—a review, *Construct. Build. Mater.* 24 (11) (2010) 2060–2071, <https://doi.org/10.1016/j.conbuildmat.2010.03.014>.
- [6] P.J. Monteiro, G. Geng, D. Marchon, J. Li, P. Alapati, K.E. Kurtis, M.J.A. Qomi, Advances in characterizing and understanding the microstructure of cementitious materials, *Cement Concr. Res.* 124 (2019), 105806, <https://doi.org/10.1016/j.cemconres.2019.105806>.
- [7] W. Li, Z. Huang, T. Zu, C. Shi, W.H. Duan, S.P. Shah, Influence of nanolimestone on the hydration, mechanical strength, and autogenous shrinkage of ultrahigh-performance concrete, *J. Mater. Civ. Eng.* 28 (1) (2016), 04015068, [https://doi.org/10.1061/\(ASCE\)MT.1943-5533.0001327](https://doi.org/10.1061/(ASCE)MT.1943-5533.0001327).
- [8] W. Li, X. Li, S.J. Chen, G. Long, Y.M. Liu, W.H. Duan, Effects of nanoalumina and graphene oxide on early-age hydration and mechanical properties of cement paste, *J. Mater. Civ. Eng.* 29 (9) (2017), 04017087, [https://doi.org/10.1061/\(ASCE\)MT.1943-5533.0001926](https://doi.org/10.1061/(ASCE)MT.1943-5533.0001926).
- [9] K. Sobolev, I. Flores, L. Torres-Martinez, P. Valdez, E. Zarazua, E. Cuellar, Engineering of SiO<sub>2</sub> Nanoparticles for Optimal Performance in Nano Cement-Based Materials, NICOM3, Springer, 2009, pp. 139–148, [https://doi.org/10.1007/978-3-642-00980-8\\_18](https://doi.org/10.1007/978-3-642-00980-8_18).
- [10] S. Kawashima, W. Li, J. Xiao, G.S. Shekhawat, S.P. Shah, Experimental investigation on quantitative nanomechanical properties of cement paste, *ACI Mater. J.* 112 (2) (2015) 229–238, <https://doi.org/10.14359/51686986>.
- [11] Z. Luo, W. Li, K. Wang, S.P. Shah, Research progress in advanced nanomechanical characterization of cement-based materials, *Cement Concr. Compos.* 94 (2018) 277–295, <https://doi.org/10.1016/j.cemconcomp.2018.09.016>.
- [12] W. Li, S. Kawashima, J. Xiao, D.J. Corr, C. Shi, S.P. Shah, Comparative investigation on nanomechanical properties of hardened cement paste, *Mater. Struct.* 49 (5) (2016) 1591–1604, <https://doi.org/10.1617/s11527-015-0597-3>.
- [13] J. Xu, D.J. Corr, S.P. Shah, Nanomechanical investigation of the effects of nanoSiO<sub>2</sub> on C-S-H gel/cement grain interfaces, *Cement Concr. Compos.* 61 (2015) 7–17, <https://doi.org/10.1016/j.cemconcomp.2015.04.011>.
- [14] X. Zhu, Y. Gao, Z. Dai, D.J. Corr, S.P. Shah, Effect of interfacial transition zone on the Young's modulus of carbon nanofiber reinforced cement concrete, *Cement Concr. Res.* 107 (2018) 49–63, <https://doi.org/10.1016/j.cemconres.2018.02.014>.
- [15] J. Xu, B. Wang, J. Zuo, Modification effects of nanosilica on the interfacial transition zone in concrete: a multiscale approach, *Cement Concr. Compos.* 81 (2017) 1–10, <https://doi.org/10.1016/j.cemconcomp.2017.04.003>.
- [16] M. Sumesh, U.J. Alengaram, M.Z. Jumaat, K.H. Mo, M.F. Alnahhal, Incorporation of nano-materials in cement composite and geopolymer based paste and mortar—A review, *Construct. Build. Mater.* 148 (2017) 62–84, <https://doi.org/10.1016/j.conbuildmat.2017.04.206>.
- [17] P.S. Deb, P.K. Sarker, S. Barbhuiya, Sorptivity and acid resistance of ambient-cured geopolymer mortars containing nano-silica, *Cement Concr. Compos.* 72 (2016) 235–245, <https://doi.org/10.1016/j.cemconcomp.2016.06.017>.
- [18] S. Riahi, A. Nazari, The effects of nanoparticles on early age compressive strength of ash-based geopolymers, *Ceram. Int.* 38 (6) (2012) 4467–4476, <https://doi.org/10.1016/j.ceramint.2012.02.021>.
- [19] A. Çevik, R. Alzebaree, G. Humur, A. Niş, M.E. Gülsan, Effect of nano-silica on the chemical durability and mechanical performance of fly ash based geopolymer concrete, *Ceram. Int.* 44 (11) (2018) 12253–12264, <https://doi.org/10.1016/j.ceramint.2018.04.009>.
- [20] T. Alomayri, Experimental study of the microstructural and mechanical properties of geopolymer paste with nano material (Al<sub>2</sub>O<sub>3</sub>), *J. Build. Eng.* 25 (2019), 100788, <https://doi.org/10.1016/j.jobe.2019.100788>.
- [21] P. Duan, C. Yan, W. Luo, W. Zhou, Effects of adding nano-TiO<sub>2</sub> on compressive strength, drying shrinkage, carbonation and microstructure of fluidized bed fly ash based geopolymer paste, *Construct. Build. Mater.* 106 (2016) 115–125, <https://doi.org/10.1016/j.conbuildmat.2015.12.095>.
- [22] H. Assaedi, F. Shaikh, I.M. Low, Characterizations of flax fabric reinforced nanoclay-geopolymer composites, *Compos. B Eng.* 95 (2016) 412–422, <https://doi.org/10.1016/j.compositesb.2016.04.007>.
- [23] S.M. Abbasi, H. Ahmadi, G. Khalaj, B. Ghasemi, Microstructure and mechanical properties of a metakaolinite-based geopolymer nanocomposite reinforced with carbon nanotubes, *Ceram. Int.* 42 (14) (2016) 15171–15176, <https://doi.org/10.1016/j.ceramint.2016.06.080>.
- [24] D. Adak, M. Sarkar, M. Maiti, A. Tamang, S. Mandal, B. Chattopadhyay, Antimicrobial efficiency of nano silver-silica modified geopolymer mortar for eco-friendly green construction technology, *RSC Adv.* 5 (79) (2015) 64037–64045, <https://doi.org/10.1039/C5RA12776A>.
- [25] M. Saafi, K. Andrew, P.L. Tang, D. McGhon, S. Taylor, M. Rahman, S. Yang, X. Zhou, Multifunctional properties of carbon nanotube/fly ash geopolymeric nanocomposites, *Construct. Build. Mater.* 49 (2013) 46–55, <https://doi.org/10.1016/j.conbuildmat.2013.08.007>.
- [26] R. Madandoust, E. Mohseni, S.Y. Mousavi, M. Namnevis, An experimental investigation on the durability of self-compacting mortar containing nano-SiO<sub>2</sub>, nano-Fe<sub>2</sub>O<sub>3</sub> and nano-CuO, *Construct. Build. Mater.* 86 (2015) 44–50, <https://doi.org/10.1016/j.conbuildmat.2015.03.100>.
- [27] W. Li, Z. Luo, C. Long, C. Wu, W.H. Duan, S.P. Shah, Effects of nanoparticle on the dynamic behaviors of recycled aggregate concrete under impact loading, *Mater. Des.* 112 (2016) 58–66, <https://doi.org/10.1016/j.matdes.2016.09.045>.
- [28] ASTM, C109/C109M-16a: Standard Test Method for Compressive Strength of Hydraulic Cement Mortars, American Society for Testing and Materials International, West Conshohocken, PA, USA, 2016.
- [29] ASTM, C1437-15, Standard Test Method for Flow of Hydraulic Cement Mortar, American Society for Testing and Materials International, West Conshohocken, PA, USA, 2015.
- [30] K.L. Scrivener, Backscattered electron imaging of cementitious microstructures: understanding and quantification, *Cement Concr. Compos.* 26 (8) (2004) 935–945, <https://doi.org/10.1016/j.cemconcomp.2004.02.029>.
- [31] S. Diamond, Considerations in image analysis as applied to investigations of the ITZ in concrete, *Cement Concr. Compos.* 23 (2–3) (2001) 171–178, [https://doi.org/10.1016/S0958-9465\(00\)00085-8](https://doi.org/10.1016/S0958-9465(00)00085-8).
- [32] Z. Luo, W. Li, Y. Gan, K. Mendu, S.P. Shah, Maximum likelihood estimation for nanoindentation on sodium aluminosilicate hydrate gel of geopolymer under different silica modulus and curing conditions, *Compos. B Eng.* 198 (2020), 108185, <https://doi.org/10.1016/j.compositesb.2020.108185>.
- [33] Z. Luo, W. Li, Y. Gan, K. Mendu, S.P. Shah, Applying grid nanoindentation and maximum likelihood estimation for NASH gel in geopolymer paste: investigation and discussion, *Cement Concr. Res.* 135 (2020), 106112, <https://doi.org/10.1016/j.cemconres.2020.106112>.
- [34] D. Davydov, M. Jirasek, L. Kopecký, Critical aspects of nano-indentation technique in application to hardened cement paste, *Cement Concr. Res.* 41 (1) (2011) 20–29, <https://doi.org/10.1016/j.cemconres.2010.09.001>.
- [35] C. Hu, Z. Li, Property investigation of individual phases in cementitious composites containing silica fume and fly ash, *Cement Concr. Compos.* 57 (2015) 17–26, <https://doi.org/10.1016/j.cemconcomp.2014.11.011>.
- [36] C. Hu, Z. Li, A review on the mechanical properties of cement-based materials measured by nanoindentation, *Construct. Build. Mater.* 90 (2015) 80–90, <https://doi.org/10.1016/j.conbuildmat.2015.05.008>.
- [37] B. Lothenbach, K. Scrivener, R. Hooton, Supplementary cementitious materials, *Cement Concr. Res.* 41 (12) (2011) 1244–1256, <https://doi.org/10.1016/j.cemconres.2010.12.001>.
- [38] J. Björnström, M. Martinelli, A. Matic, L. Börjesson, I. Panas, Accelerating effects of colloidal nano-silica for beneficial calcium–silicate–hydrate formation in cement, *Chem. Phys. Lett.* 392 (1–3) (2004) 242–248, <https://doi.org/10.1016/j.cplett.2004.05.071>.
- [39] J. Chen, S.-c. Kou, C.-s. Poon, Hydration and properties of nano-TiO<sub>2</sub> blended cement composites, *Cement Concr. Compos.* 34 (5) (2012) 642–649, <https://doi.org/10.1016/j.cemconcomp.2012.02.009>.
- [40] E. Berodier, K. Scrivener, Understanding the filler effect on the nucleation and growth of C-S-H, *J. Am. Ceram. Soc.* 97 (12) (2014) 3764–3773, <https://doi.org/10.1111/jace.13177>.
- [41] B.Y. Lee, K.E. Kurtis, Influence of TiO<sub>2</sub> nanoparticles on early C<sub>3</sub>S hydration, *J. Am. Ceram. Soc.* 93 (10) (2010) 3399–3405, <https://doi.org/10.1111/j.1551-2916.2010.03868.x>.
- [42] E. García-Taengua, M. Sonebi, K. Hossain, M. Lachemi, J. Khatib, Effects of the addition of nanosilica on the rheology, hydration and development of the compressive strength of cement mortars, *Compos. B Eng.* 81 (2015) 120–129, <https://doi.org/10.1016/j.compositesb.2015.07.009>.
- [43] C.A. Rees, J.L. Provis, G.C. Lukey, J.S. Van Deventer, The mechanism of geopolymer gel formation investigated through seeded nucleation, *Colloids Surf., A* 318 (1–3) (2008) 97–105, <https://doi.org/10.1016/j.colsurfa.2007.12.019>.
- [44] P.S. Deb, P.K. Sarker, S. Barbhuiya, Effects of nano-silica on the strength development of geopolymer cured at room temperature, *Construct. Build. Mater.* 101 (2015) 675–683, <https://doi.org/10.1016/j.conbuildmat.2015.10.044>.
- [45] J.W. Phair, J. Van Deventer, J. Smith, Mechanism of polysialylation in the incorporation of zirconia into fly ash-based geopolymers, *Ind. Eng. Chem. Res.* 39 (8) (2000) 2925–2934, <https://doi.org/10.1021/ie990929w>.
- [46] J.J. Chen, L. Sorelli, M. Vandamme, F.J. Ulm, G. Chanvillard, A Coupled nanoindentation/SEM-EDS study on low water/cement ratio Portland cement paste: evidence for C-S-H/Ca(OH)<sub>2</sub> nanocomposites, *J. Am. Ceram. Soc.* 93 (5) (2010) 1484–1493, <https://doi.org/10.1111/j.1551-2916.2009.03599.x>.

- [47] Z. Zhang, J.L. Provis, A. Reid, H. Wang, Fly ash-based geopolymers: the relationship between composition, pore structure and efflorescence, *Cement Concr. Res.* 64 (2014) 30–41, <https://doi.org/10.1016/j.cemconres.2014.06.004>.
- [48] M. Zou, D. Yang, Nanoindentation of silica nanoparticles attached to a silicon substrate, *Tril.* 22 (2) (2006) 189–196, <https://doi.org/10.1007/s11249-006-9079-7>.
- [49] I. Gheewala, R. Smith, S. Kenny, Nanoindentation and nanoscratching of rutile and anatase  $\text{TiO}_2$  studied using molecular dynamics simulations, *J. Phys. Condens. Matter* 20 (35) (2008), 354010, <https://doi.org/10.1088/0953-8984/20/35/354010>.
- [50] O. Zywitzki, T. Modes, H. Sahm, P. Frach, K. Goedicke, D. Glöß, Structure and properties of crystalline titanium oxide layers deposited by reactive pulse magnetron sputtering, *Surf. Coating. Technol.* 180 (2004) 538–543, <https://doi.org/10.1016/j.surfcoat.2003.10.115>.
- [51] H.M. Jennings, J.J. Thomas, J.S. Gevrenov, G. Constantinides, F.-J. Ulm, A multi-technique investigation of the nanoporosity of cement paste, *Cement Concr. Res.* 37 (3) (2007) 329–336, <https://doi.org/10.1016/j.cemconres.2006.03.021>.
- [52] G. Constantinides, F.-J. Ulm, The nanogranular nature of C-S-H, *J. Mech. Phys. Solid.* 55 (1) (2007) 64–90, <https://doi.org/10.1016/j.jmps.2006.06.003>.